Design and performance of a vacuum-UV simulator for material testing under space conditions

M. Sznajder[a], T. Renger[b,*], A. Witzke[b], U. Geppert[b,c], R. Thornagel[d]

[a] *DLR Institute for Space Systems, University of Bremen, Robert Hooke Str. 7, 28359 Bremen, Germany*
[b] *DLR Institute for Space Systems, System Conditioning, Robert Hooke Str. 7, 28359 Bremen, Germany*
[c] *Kepler Institute of Astronomy, University of Zielona Góra, 65-265 Zielona Góra, Lubuska 2, Poland*
[d] *Physikalisch-Technische Bundesanstalt, Abbestr. 2-12, 10587 Berlin, Germany*

Abstract

This paper describes the construction and performance of a VUV-simulator that has been designed to study degradation of materials under space conditions. It is part of the Complex Irradiation Facility at DLR in Bremen, Germany, that has been built for testing of material under irradiation in the complete UV-range as well as under proton and electron irradiation. Presently available UV-sources used for material tests do not allow the irradiation with wavelengths smaller than about 115 nm where common Deuterium lamps show an intensity cut-off. The VUV-simulator generates radiation by excitation of a gas-flow with an electron beam. The intensity of the radiation can be varied by manipulating the gas-flow and/or the electron beam.

The VUV simulator has been calibrated at three different gas-flow settings in the range from 40 nm to 410 nm. The calibration has been made by the Physikalisch-Technische Bundesanstalt (PTB) in Berlin. The measured spectra show total irradiance intensities from 24 to 58 mWm^{-2} (see Table 4.2) in the VUV-range, i.e. for wavelengths smaller than 200 nm. They exhibit a large number of spectral lines generated either by the gas-flow constituents or by metal atoms in the residual gas which come from metals used in the source construction. In the range from 40 nm to 120 nm where Deuterium lamps are not usable, acceleration factors of 3 to 26.3 Solar Constants are reached depending on the gas-flow setting. The VUV-simulator allows studies of general degradation effects caused by photoionization and photodissociation as well as accelerated degradation tests by use of intensities that are significantly higher compared to that of the Sun at 1 AU.

Keywords: material testing, UV degradation, VUV

1. Introduction

All materials planned for space applications in which they will be exposed to the radiation in space have to be evaluated for their behavior under particle and UV radiation (ASTM, E512, 2010; ECSS, 2008). It is known from many of these evaluation tests that particle and UV radiation can significantly degrade materials and, e.g. lead to changes in their mechanical behavior or thermo-optical properties (Agnolan, 2007; Heltzel et al., 2009; Lura et al., 2002; Marco et al., 2009; Romero & Boscher, 1998; Sharma & Sridhara, 2012). These changes can cause early failures of satellite components or even failures of complete space missions (Dachwald, 2005).

This paper discusses the design and performance of a radiation source that has been developed to simulate the short wavelength part of the Vacuum-UV region of the solar spectrum during material tests. The solar UV radiation is generally defined as the solar radiation with wavelengths from 10 nm to 400 nm (ASTM, E512, 2010). The range between 200 nm and 400 nm is named Near-UV (NUV) range. The other part of the solar UV radiation from 10 nm to 200 nm is denoted as the Vacuum-UV (VUV) range. Extraterrestrial intensity spectra of both ranges show that the contribution of the VUV radiation to the total intensity of solar UV irradiation is almost negligible (Fig. 1). The VUV-irradiation amounts to only 0.1% of the NUV irradiation intensity. However, the VUV radiation can noticeably contribute to the degradation of materials despite of its small amount of total intensity. The energy of a single photon in the VUV range is considerably higher compared to a photon in the NUV range. VUV-photon energies vary from 6 eV to 124 eV whereas NUV-photon energies range only from 3 eV to 6 eV. Therefore, VUV radiation can generate photoionization and photodissociation effects that cannot be caused by the significantly lower photon energies in the NUV range. Thus, degradation effects that would not occur under NUV irradiation even at very high intensities may be expected if the material is exposed to VUV irradiation for longer periods of time.

To get the most reliable information on UV degrada-

*Corresponding author
Email address: Thomas.Renger@dlr.de (T. Renger)

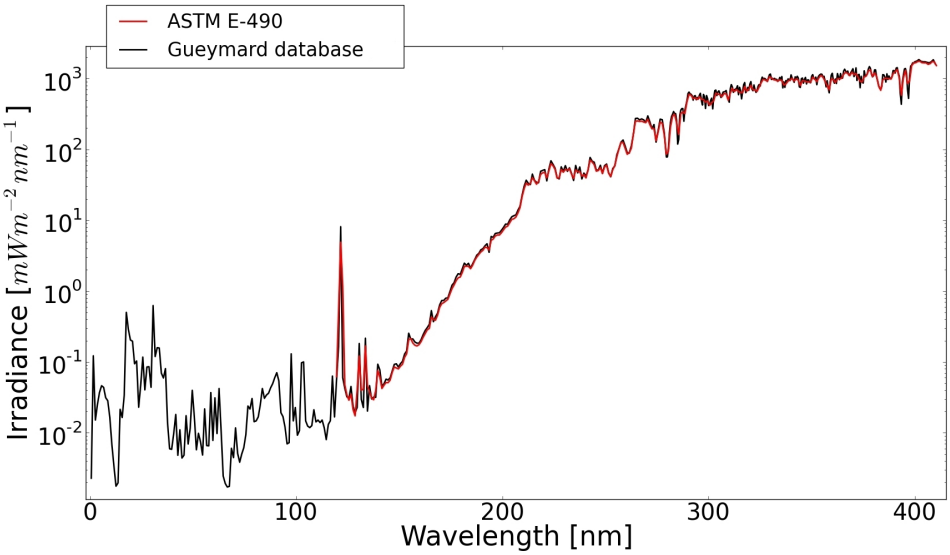

Figure 1: Extraterrestrial spectral solar UV-irradiance at 1 AU (astronomic unit). The red line shows data from ASTM E-490 (ASTM, E490, 2006). This standard provides data only down to 119.5 nm. The black line exhibits spectral data from Gueymard (Gueymard, 2004). This data are representative for average solar activity conditions. They are in very good accordance to the ASTM E-490 spectrum between 120 nm and 400 nm.

tion of materials in space by ground material tests, the UV-spectrum of the Sun should be simulated as close as possible. The NUV spectral region can be simulated by using commercial short arc Xenon lamps (Marco & Remaury, 2004). The VUV spectral range is simulated with Deuterium lamps in almost all material tests (e.g. Polsak et al., 2003). These lamps, however, feature a lower wavelength cut-off at approx. 115 nm due to internal MgF_2- or LiF_2-windows which exhibit a strong decrease in transmission at this wavelength. This leads to the fact that the residual VUV wavelength range between 10 nm and 115 nm is generally not covered in up-to-date material tests although especially this range shows a strong increase of photon energies from 10 eV to 124 eV.

In context with the installation of the new Complex Irradiation Facility (CIF) for material testing at the German Aerospace Center (DLR) (Renger T. et al., 2012, 2014) which should be capable of simulating the complete solar UV irradiation as well as proton and electron irradiation, the lack in the VUV simulation of the solar spectrum by currently available radiation sources necessitated the construction of a VUV simulator that covers the range from 10 nm to at least 115 nm. Beside a good approximation to the real solar spectrum this simulator has to achieve several other requirements to make it useful for material testing: It has to exceed the radiation intensity of the Sun (at 1 AU) at the sample area of the CIF in order to accelerate the degradation of the tested materials and to allow the simulation of long-term effects. Furthermore, the simulator has to generate radiation that is emitted under a relatively large solid angle into the test chamber to permit the simultaneous irradiation of several samples with a homogenous intensity distribution. It must, moreover, be capable of working continuously during a sufficiently long period of time. The construction must take into account that the VUV simulator has to be connected to the test chamber without any window as no window material is known that completely transmits radiation in the concerned spectral range. Therefore, the design has to ensure that no significant amount of particles of the medium necessary to generate the radiation can migrate inside the test chamber.

Below we describe in detail the design and performance of a VUV simulator that has been built with regard to the given requirements above. It bases on a design of a VUV gas-jet simulator that was constructed 15 years ago by the Institute of Low Temperature Physics and Engineering in Kharkov, Ukraine, in collaboration with the DLR (Verkhovtseva at al., 1997). The calibration of the VUV simulator has been carried out in the range from 40 nm to 410 nm by the Physikalisch Technische Bundesanstalt (PTB) in Berlin, Germany. The calibration method and procedure is briefly explained in Section 3. The spectral distribution of radiation as well as the irradiance, the derived acceleration factors as well as the stability of the source are discussed and summarized in the ensuing Sections 4.1, 4.2 and 4.3. The summary is given in Section 5.

2. Design and Principle of Operation of the VUV-Source

The design of the VUV simulator is based on the semicryogenic version of the previous simulators which are described in (Verkhovtseva at al., 1997). The radiation is

produced by the transition of electrons belonging to excited gas atoms into their ground state. The gas atoms are excited by electron bombardment of a spatially limited supersonic gas jet which flows into a vacuum chamber. The vacuum is maintained by a combination of cryogenic and mechanical pumps (semi-cryogenic design). A pressure of about 1 mbar inside the jet is sufficient for an effective excitation. Beyond the jet close to its boundary the gas pressure is several orders less (10^{-4} mbar) caused by the supersonic directional motion of the jet. This is the premise to locate an electron source in the close vicinity of the gas jet. This method generates electromagnetic radiation in a broad spectral range (soft X-rays, VUV, NUV) with relatively high intensities at lower wavelengths (< 115 nm) and permits a design without windows, which would disable the transmission in this range. The spectral intensity distribution of the radiation depends on the gas mixture, the flow rate of the jet, the electron current (on the alignment between beam and jet, and the focus of the electron beam).

Fig. 2 illustrates the arrangement of the electron source and the gas jet inside the vacuum chamber of the simulator. The outlet of the generated VUV-light is realized behind the spot perpendicular to the figures plane. The electrons which pass through the gas jet are caught by the collector at the opposite side of the source. The components of the vacuum system are better visible in Fig. 3, whose plane is perpendicular to the plane of Fig. 2.

The gas jet is injected by a nozzle from top of the VUV-chamber into the vacuum. The flow rate is stabilized by a flow controller and is adjustable by software in the range between 0 and 5000 sccm (standard cubic centimeter per minute). The bulk of the gas load is pumped out through an intake port at the bottom of the chamber by a screw pump. The rest, which is a small fraction of about 3% is removed by cryogenic condensation at two baffles. Each of them is connected to one of the both stages of the cold head of a commercial cryogenic pump (Helium cooling machine). The 2^{nd} stage reaches a bottom temperature of 15 K without gas load. It increases to about 20 K under gas load by formation of ice, which decreases the pumping power gradually and limits the operating time. The temperature is logged permanently as an indicator when a regeneration is necessary to remove the ice. During this process the cryogenic pump is turned off while the mechanical pumps continue their operation. The temperature inside the chamber increases and the residual gas, which is frozen on the cold baffles, is pumped out. The gas nozzle is thermally connected to a water circuit for tempering it to avoid a freeze. The combination of both pumping procedures is possible due to the effect that the gas inside the intake port banks itself. Thereby, a reverse flow from the pipeline is impeded and the pressure regions are separated by 10^{-4} mbar around the gas jet (inside the chamber) and more than 10^{-2} mbar inside the pipeline.

A differential pumping segment is installed at the light outlet consisting of a turbomolecular pump and an aperture assembly. It improves the pressure conditions inside the radiation chamber and reduces the metal traces to the lowest possible limit. Since tests can be performed in the chamber at pressures of 10^{-6} mbar and less the pollution by metals over the test period is expected to be negligible. The fraction of light which is permitted to the test chamber is colored yellow in Fig. 3. An opening angle of about 6^{o} is defined by the apertures in the cryogenic baffles and at the differential pumping segment. It ensures the irradiation of a target area with a diameter of 80 mm at a distance of about 770 mm from the spot, as it is realized in CIF. To avoid that charged particles produced at the spot can reach the irradiated object, an electric filter is installed at the light outlet, which deflects them beyond the radiation flow.

The axes of the gas jet, the electron beam and the light outlet are arranged out of square, while the orientation of the light outlet is horizontal. The axis of the gas jet is turned by 15^{o} to the vertical axis in the direction of the light outlet. The electron beam is inclined by 15^{o} to the horizontal axis but in its vertical plane it is perpendicular to the light outlet. The idea of this design is that the probability that particles could reach the radiation chamber or damage the cathode of the electron source is less than for a perpendicular arrangement.

The electron source is realized as a Pierce-type model with a magnetic lens behind the anode. The LaB_6-cathode is heated up electrically by adjusting the cathode voltage depending on which emission current is needed. The electronic control unit of the source provides a PID algorithm which stabilizes the emission current by varying the Wehnelt voltage automatically. The beam is focused by setting the current for the magnetic lens.

Two flanges are located at the opposite side of the light outlet. Each is connected with a window for visual inspection of the luminous jet and with a radiation indicator compartment (see Fig. 3). The indicator measures the signal of the source. The digital value of the signal is visualized by the controlling software to monitor the stability of the radiation. During the calibration procedure for every measured spectrum the corresponding sensor value has been determined.

Fig. 4 illustrates the size and intensity of the spot qualitatively with different settings for the emission current and for the gas flow. The photos were taken through the window at the opposite side of the light outlet (see Fig. 3).

Based on the experience of the first design of the VUV simulator (Verkhovtseva at al., 1997), the same gas mixture has been chosen to produce the spectra. The mixture provides a continuum spectrum similar to the Sun's spectrum. Due to the presence of the water particles in the chamber the Hydrogen Lyman α as well as the other H lines are present (see Figs. 6 and 7). The intensity of the VUV light increases generally up to a saturation value with increasing gas flow. An increasing gas flow, however, reduces the quality of the vacuum in the radiation chamber.

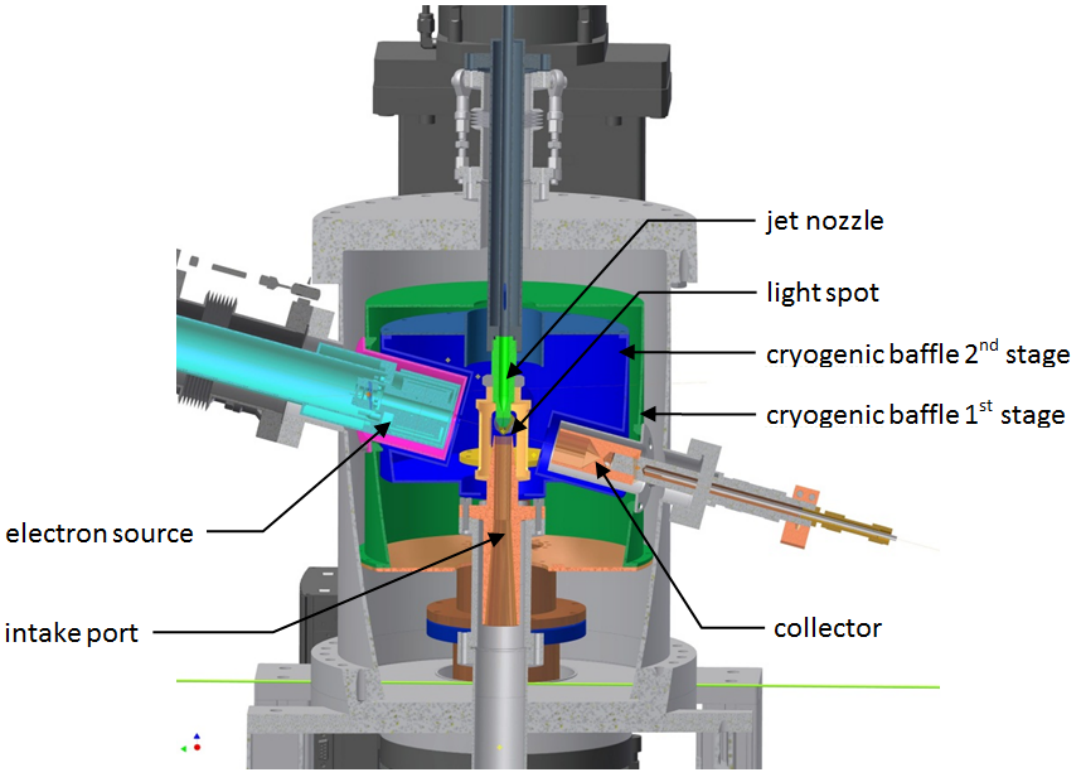

Figure 2: Sectioning of the VUV-simulator along the electron beam.

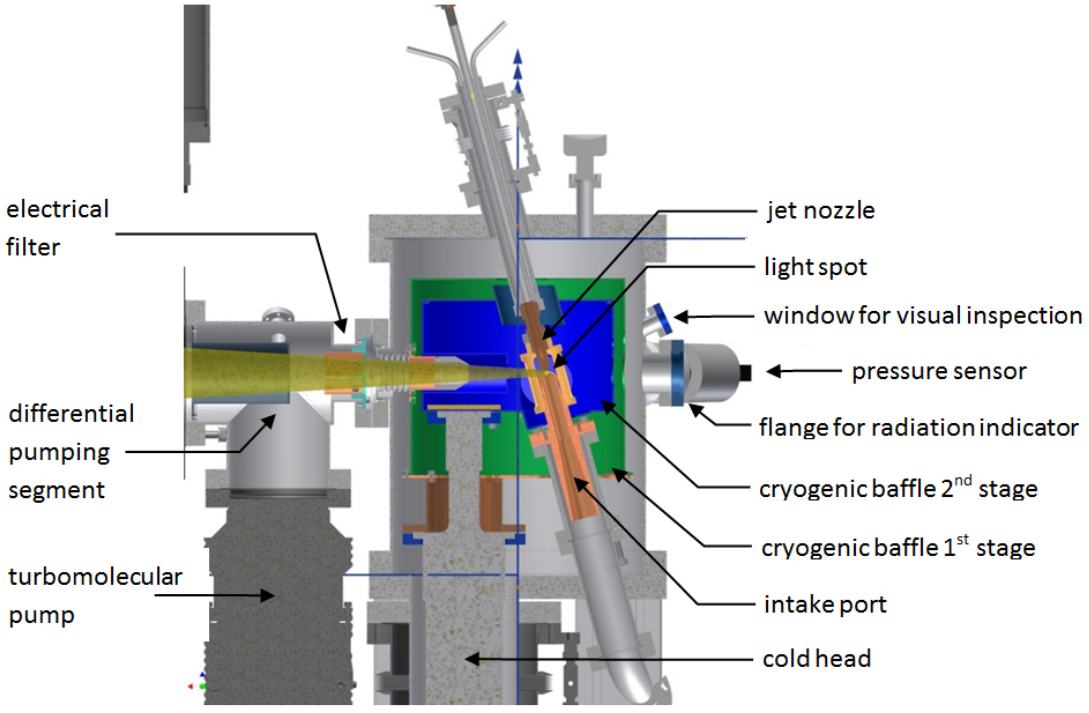

Figure 3: Sectioning of the VUV-simulator along the light outlet (yellow).

Thus, the sensitive balance between VUV light intensity and vacuum quality has to be taken into account when optimizing the VUV source parameters. In the same way, a larger emission current causes, for a given gas flow, a

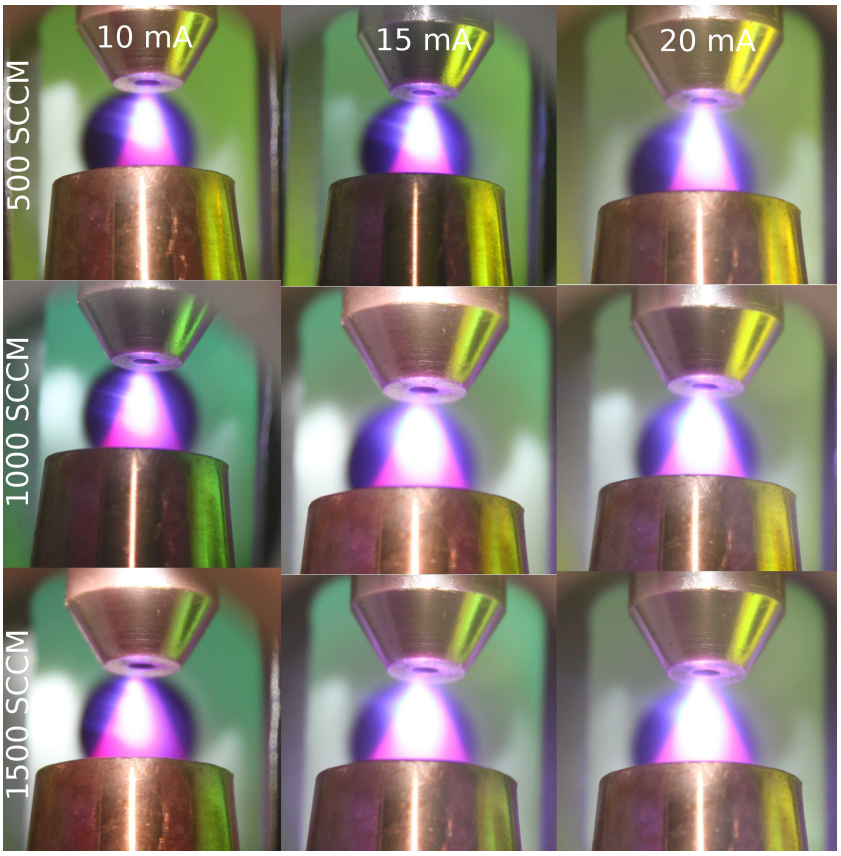

Figure 4: Pictures of the VUV-spot with different settings of the gas flow rate (rows: 500, 1000 and 1500 sccm) and the emission current (columns: 10, 15 and 20 mA).

higher intensity of the radiation. Therefore it is favorable to operate the simulator with relatively small gas flows and high electron currents to get the same intensity.

After first function tests concerning the stability and operating life, the following settings were chosen for the calibration procedure:

- Gas mixture: Ar (98.5%), Kr (1%) and He (0.5%)
- Electron energy: 1 keV,
- Electron emission current: 20 mA,
- Flow rate of the gas jet: 300, 600, 1200 sccm.

The goals for the calibration procedure were:

1. Finding the optimal alignment between electron beam and gas jet,
2. Finding the magnetic lens current for an optimal focus of the electron beam,
3. Measurement of the spectral radiant intensity of the radiation.

3. The method and procedure of calibration

The VUV source was calibrated in the radiometry laboratory of the Physikalisch-Technische Bundesanstalt (PTB) at Berlin Electron Storage Ring for Synchrotron Radiation of Helmholtz Zentrum Berlin (BESSY II) in Berlin-Adlershof. PTB provides the calibration of radiation detectors and sources as well as the characterization of optical components in the UV and VUV range (Richter et al., 2001; Richter & Ulm, 1999).

Fig. 5 shows the normal-incidence monochromator (1m, 15° McPherson type) beam line for source calibration in the configuration for the calibration of the measurement site, where synchrotron radiation is used as a primary source standard.

The whole device can be rotated around the entrance axis to take the polarization of synchrotron radiation into account during that procedure. Moreover, it is possible to shift the monochromator compartment via linear bearings perpendicular to the entrance axis in order to connect it with the light outlet of the source to be calibrated.

The toroidal mirror (see Fig. 5) images the light spot into the entrance slit of the monochromator. The solid angle of accepted radiation is precisely defined by apertures (not shown in Fig. 5). A spherical grating maps the entrance slit in the first spectral order into the exit slit, where the radiation of the selected wavelength is detected by a photomultiplier tube. The corresponding wavelength and the spectral resolution depend on the angular position of

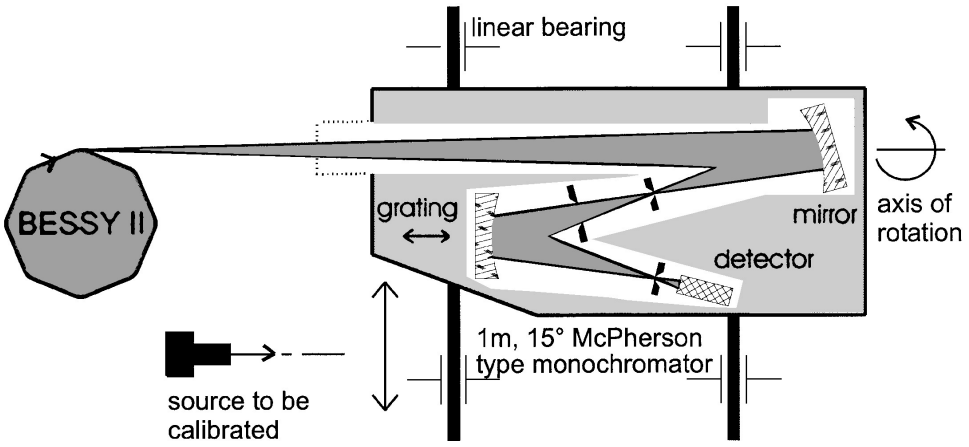

Figure 5: The normal - incidence monochromator beam line used for calibration of radiation sources (Richter et al., 2001).

the grating, the grating constant, the slit width, and other parameters, which are optimized in order to suppress the influence of higher spectral order too. The measurement of the spectral radiant intensity is performed by varying the angle of the grating in different spectral ranges with a given resolution (wavelength scan). Additionally, it is possible to vary the angle of the toroidal mirror to measure the intensity at different horizontal and vertical positions at a fixed wavelength (in combination with appropriate apertures and slits) to record a spatial profile of the radiating spot and to align the image of the spot into the entrance slit of the monochromator. Four monochromator configurations were used to calibrate the VUV-simulator in the following spectral ranges with given resolutions:

- 40 nm to 120 nm, resolution: 0.2 nm,
- 110 nm to 220 nm, resolution: 0.2 nm,
- 160 nm to 330 nm, resolution: 1 nm,
- 300 nm to 410 nm, resolution: 1 nm.

The first step for the calibration of the VUV-simulator was the alignment to the entrance axis of the monochromator and the connection of the vacuum systems of both facilities. After first wavelength scans in the range between 110 nm and 220 nm a relatively intense spectral line was chosen for the alignment of the electron beam to the gas jet. That means, the monochromator was adjusted to that intense wavelength (e.g. 123.62 nm) and the orientation of the electron source and the gas nozzle were changed during the timely monitoring of the detector signal to find the optimum. The same procedure was performed for the setting of the magnetic lens current. After that, the wavelength scans were performed with the settings of the VUV-simulator described in Section 2 in the spectral ranges given above.

4. The VUV spectra, comparison to the solar spectra

4.1. Spectral intensity distribution

In order to get the spectral radiant intensity in W sr^{-1} nm^{-1}, the measured detector signals in the described wavelength ranges were converted with the corresponding measurement site sensivity by PTB. By use of the geometrical parameters of the CIF that spectral radiant intensity was re-calculated into spectral irradiance at the position of the object under test in W m^{-2} nm^{-1}. Since for each parameter setting several measurements have been performed, an averaged spectral distribution was calculated (see Section 4.3).

The resulting spectral irradiance distributions are shown in Figs. 6-9 for each gas flow (300, 600, 1200 sccm) with a different colour. The integral irradiance for each configuration of the VUV-source is given in the legend. A survey of all spectra over the whole range from 40 to 410 nm is presented in Fig. 10.

The spectra of the VUV-simulator are characterized by a large number of lines. The verification of these spectral lines was made by use of the database of the National Institute of Standards and Technology (NIST) (Ralchenko et al., 2011). Each identified spectral line is marked in Figs. 6-9 by a label which contains the name of the chemical element and the degree of ionization. An overview of all identified spectral lines is presented in the Appendix (Table A.1).

Spectral lines in the wavelength range from 138 nm to 160 nm are classified separately (see Fig. 7 and Table A.2). For larger gas flows the spectral lines in that range disappear and large bumps appear. This is an effect of the increasing number of collisions between the gas atoms. That result in a broadening of the spectral lines which form eventually a continuum. The NIST database possesses in this wavelength range 112 Ar lines, 140 Kr lines and no He lines.

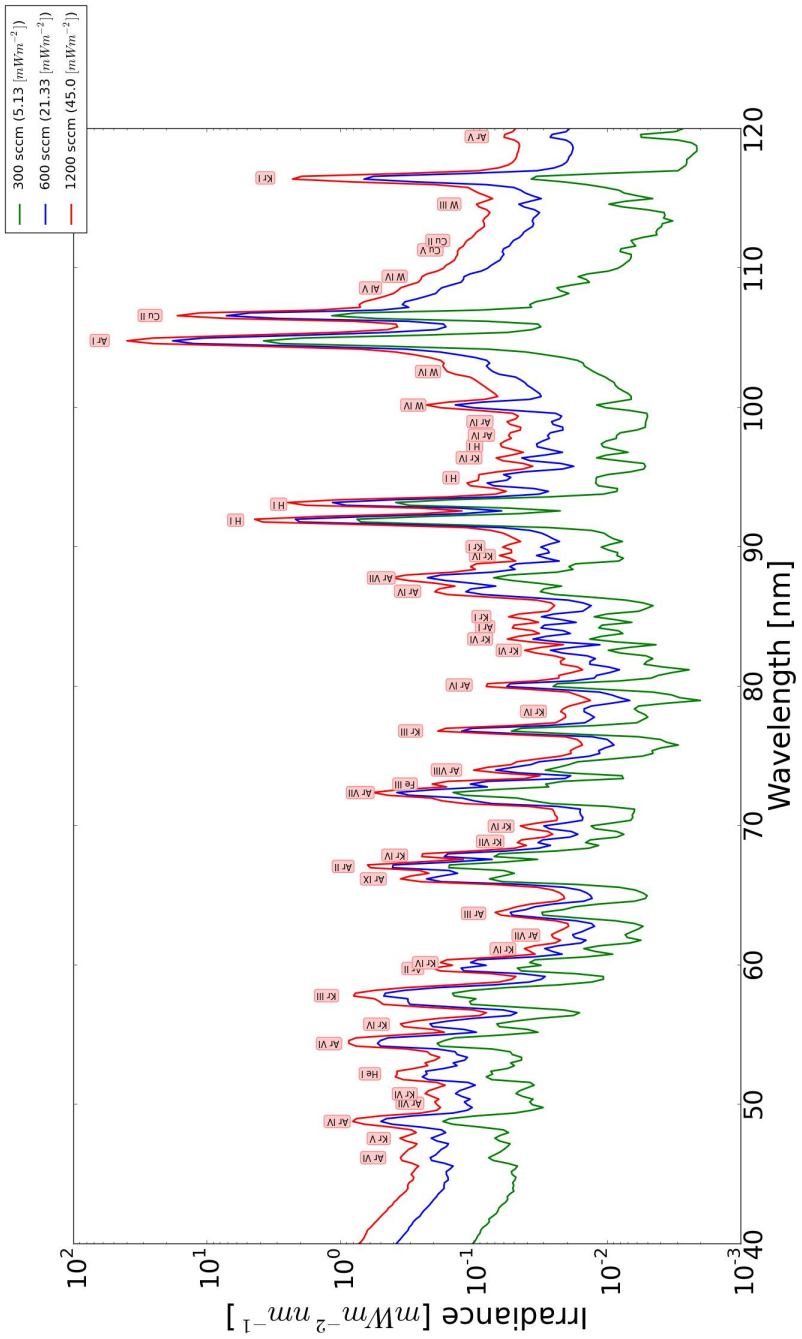

Figure 6: The VUV spectral lines in the wavelength range from 40 nm to 120 nm for different gas flows: 300 (green line), 600 (blue line) and 1200 (red line).

In order to get an idea how good the VUV-source simulates the solar spectrum, the appearance of solar spectral lines and their possible counterparts of the VUV-simulator has to be studied.

Since the ASTM E-490 standard of the spectral solar emissivity covers the wavelength range from 119.5 nm to 1000000 nm, the Gueymard database (Gueymard, 2004) is used as a reference for wavelengths < 120nm. The VUV-simulator spectrum and the Gueymard standard are shown in Fig. 11. From 119.5 nm to 150 nm the VUV-simulator spectrum coincides well with the solar emission lines. Below 119.5 nm the spectral intensity of the VUV-simulator

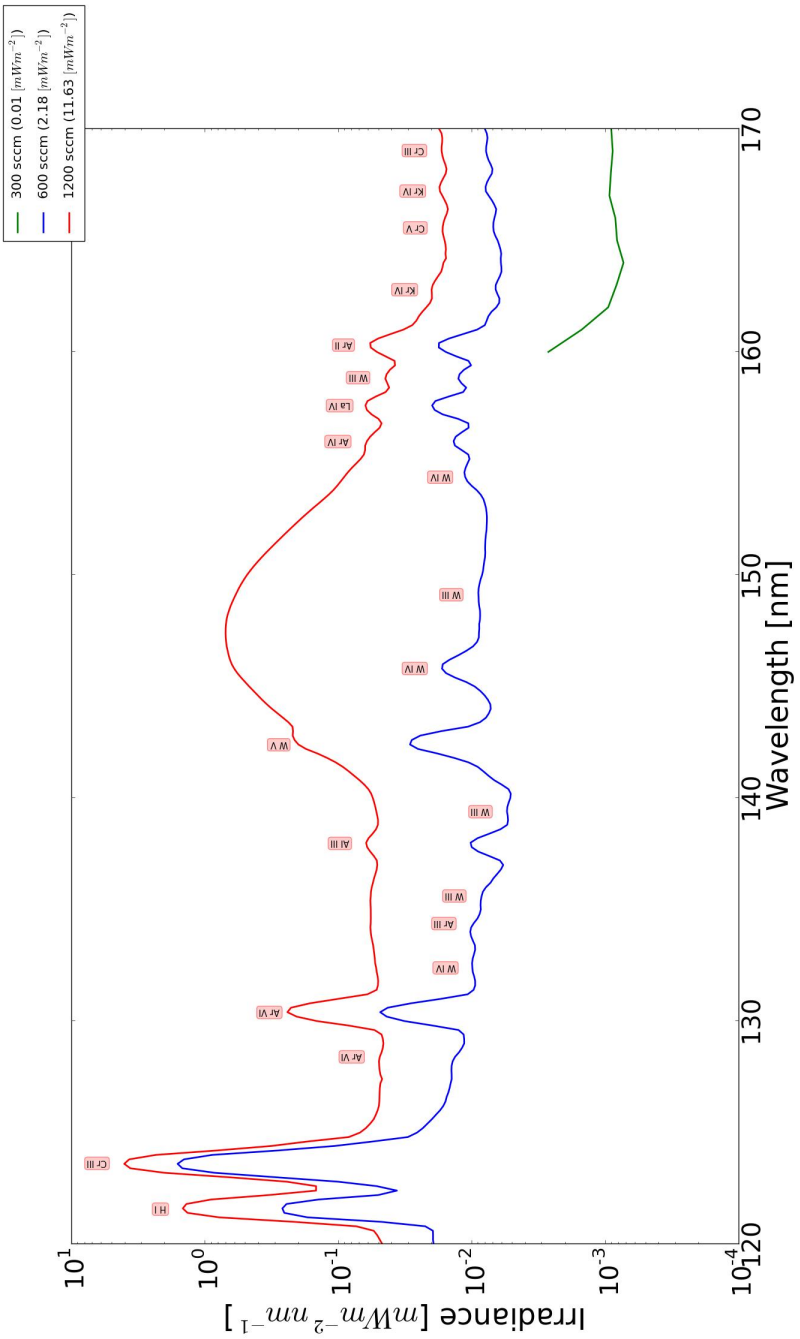

Figure 7: The VUV spectral lines in the wavelength range from 120 nm to 170 nm for different gas flows: 300 (green line), 600 (blue line), 1200 (red line).

is larger than the solar one. Since the VUV-source has a very small intensity for wavelengths above 150 nm, this range must be covered by the light of a Deuterium lamp - another light source of the CIF.

To compare the VUV-simulator emission lines with the solar ones, the SUMER database (Curdt et al., 2004) has been chosen as a reference. A Lyman-α line at 121.57 nm has been identified both in the spectrum of the VUV-simulator and in (Curdt et al., 2004). Its intensity in the spectrum of the VUV-simulator is 18% of the corresponding solar one. Strong Hydrogen lines of the VUV source are present at: 91.93 nm (131 times stronger-), 93.07 nm

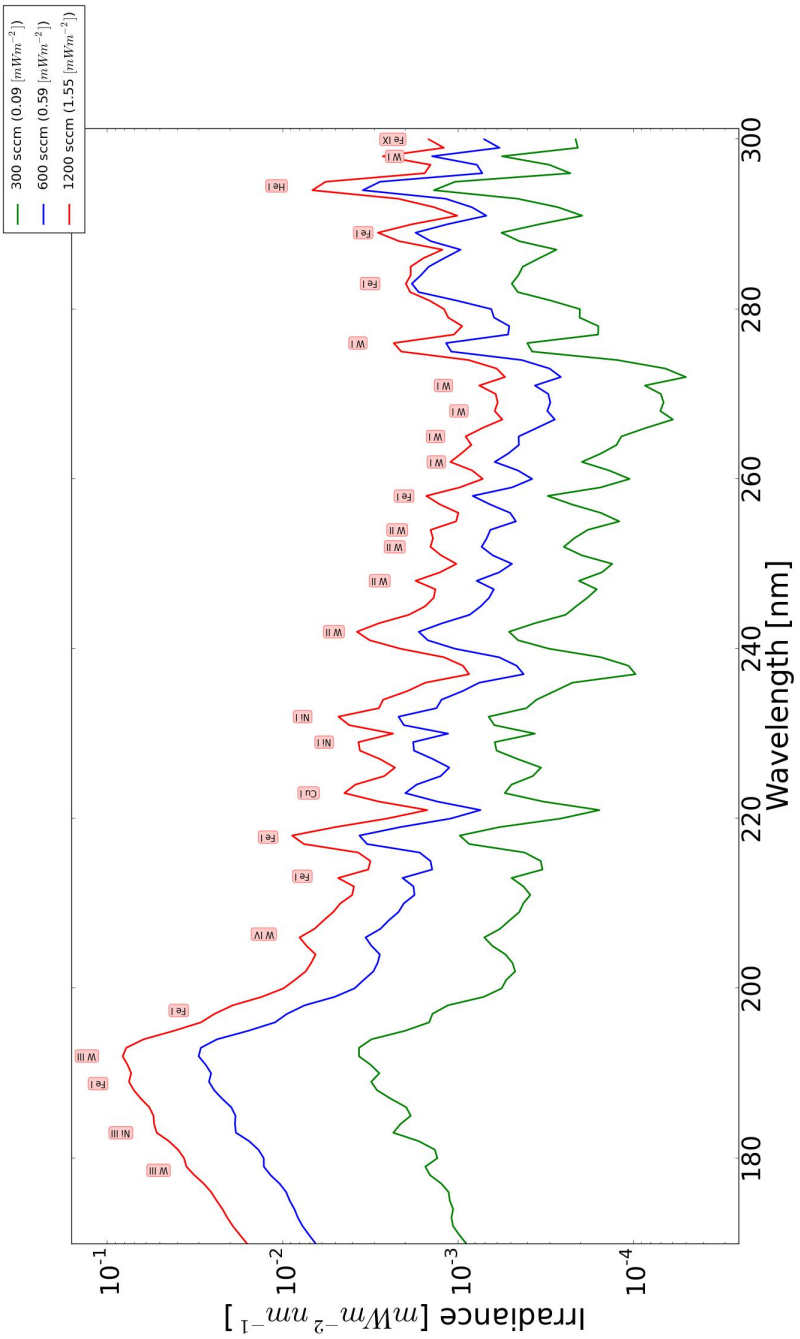

Figure 8: The VUV spectral lines in the wavelength range from 170 nm to 300 nm for different gas flows: 300 (green line), 600 (blue line), 1200 (red line).

(138 times stronger-), and 94.97 nm (10 times stronger-than the Sun spectrum at that wavelengths). The presence of Hydrogen and residual water vapor in the VUV-simulator is a consequence of the fact, as it is the predominant residual gas in metal vacuum systems at very low pressures (Redhead P. A., 2002). The two strongest lines of the VUV-source spectrum appear at 104.82 nm and 106.61 nm. They correspond to the Ar I and Cu II lines that are 2922 - times and 1423 - times stronger than the solar spectrum at these wavelengths. In the solar spectrum these lines are not present. Also not present in the solar spectrum are the VUV-source lines at 123.62 nm and

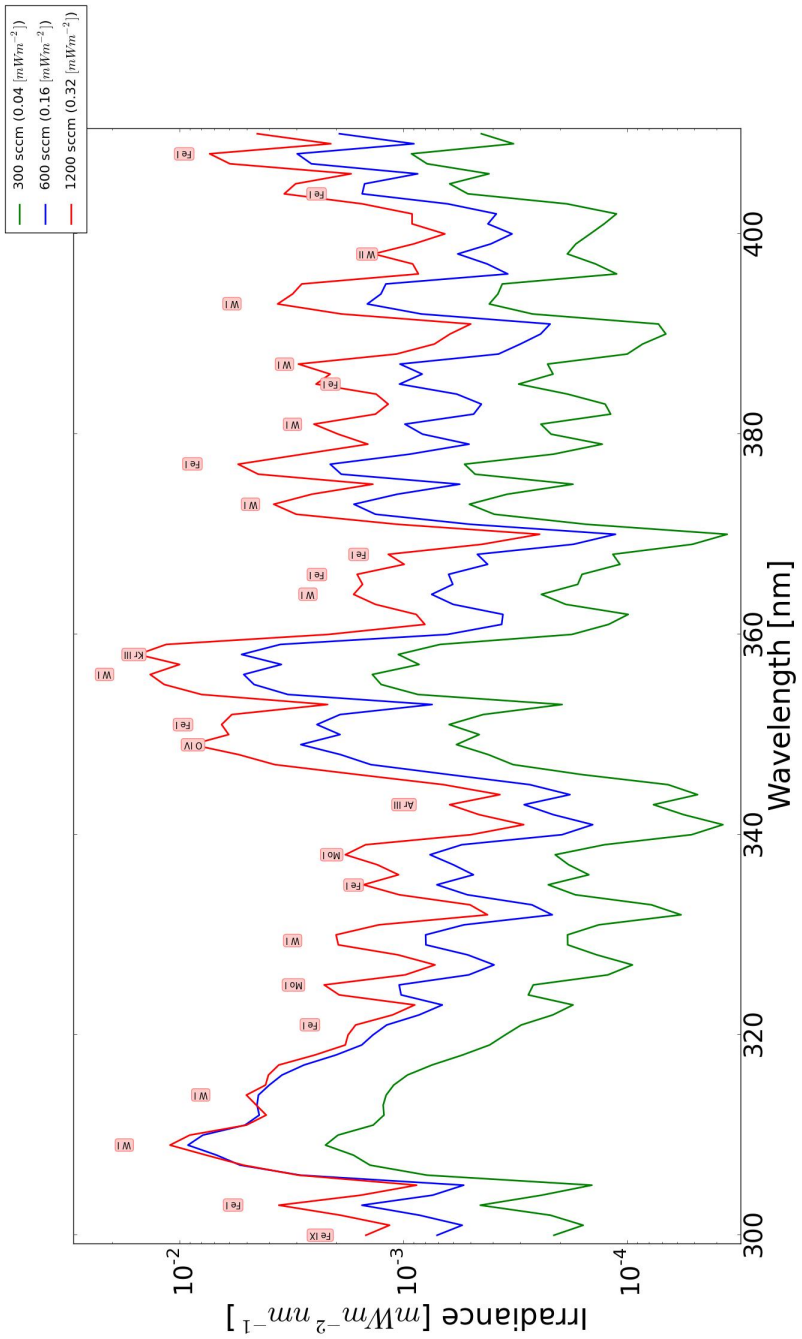

Figure 9: The VUV spectral lines in the wavelength range from 300 nm to 410 nm for different gas flows: 300 (green line), 600 (blue line), 1200 (red line).

116.49 nm (Kr I and Cr III). The Ar- Kr- and He-lines are caused by constituents of the gas flow excited by the electron beam. The metal lines such as: Cu, Cr, W, Fe, Mo, Ni, La and Al originate from the construction materials of the VUV-simulator. These lines are constituents of the solar spectrum too (Curdt et al., 2004).

4.2. Acceleration factors

The acceleration factor of material tests for space application is generally defined as the ratio of the intensity of a degrading radiation applied to a material at the laboratory versus the intensity of the same degrading factor in space (ECSS, 2008). In the following the acceleration fac-

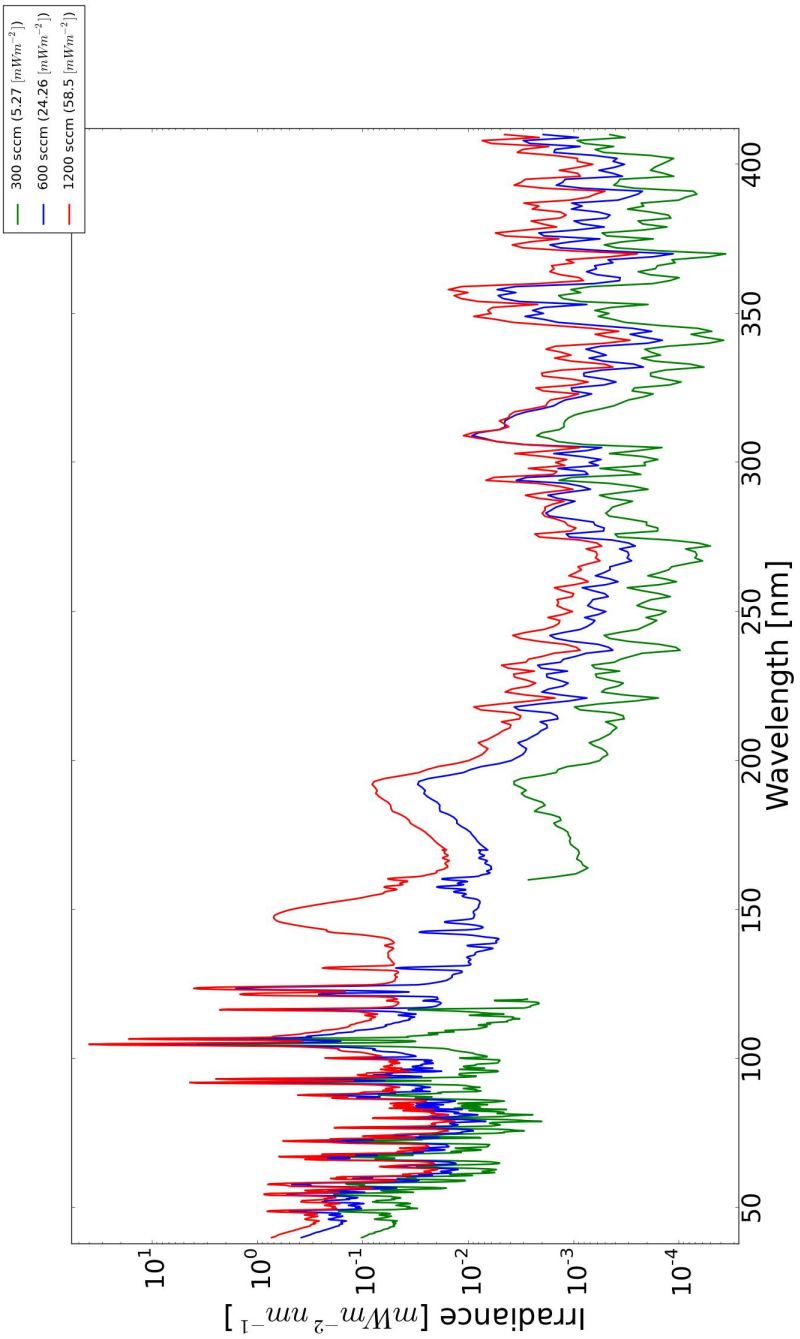

Figure 10: Summary plot of the VUV spectra in the wavelength range from 40 nm to 410 nm for different gas flows: 300 (green line), 600 (blue line), 1200 sccm (red line).

tors achieved by the VUV-simulator are discussed. They are calculated as the ratio of its intensity in a certain spectral range to the intensity of the solar radiation in the same range at 1 AU. The factors decrease if materials are tested for space applications that go closer to the Sun, whereas the factors increase in the case of applications that veer away from the Sun.

The differential as well as integrated values of the Gueymard's and VUV-simulator's spectral intensities and acceleration factors are presented in Tables 4.1 and 4.2, respectively. The highest differential acceleration factor of 95.4 SC is reached in the wavelength range 100 nm to 110 nm

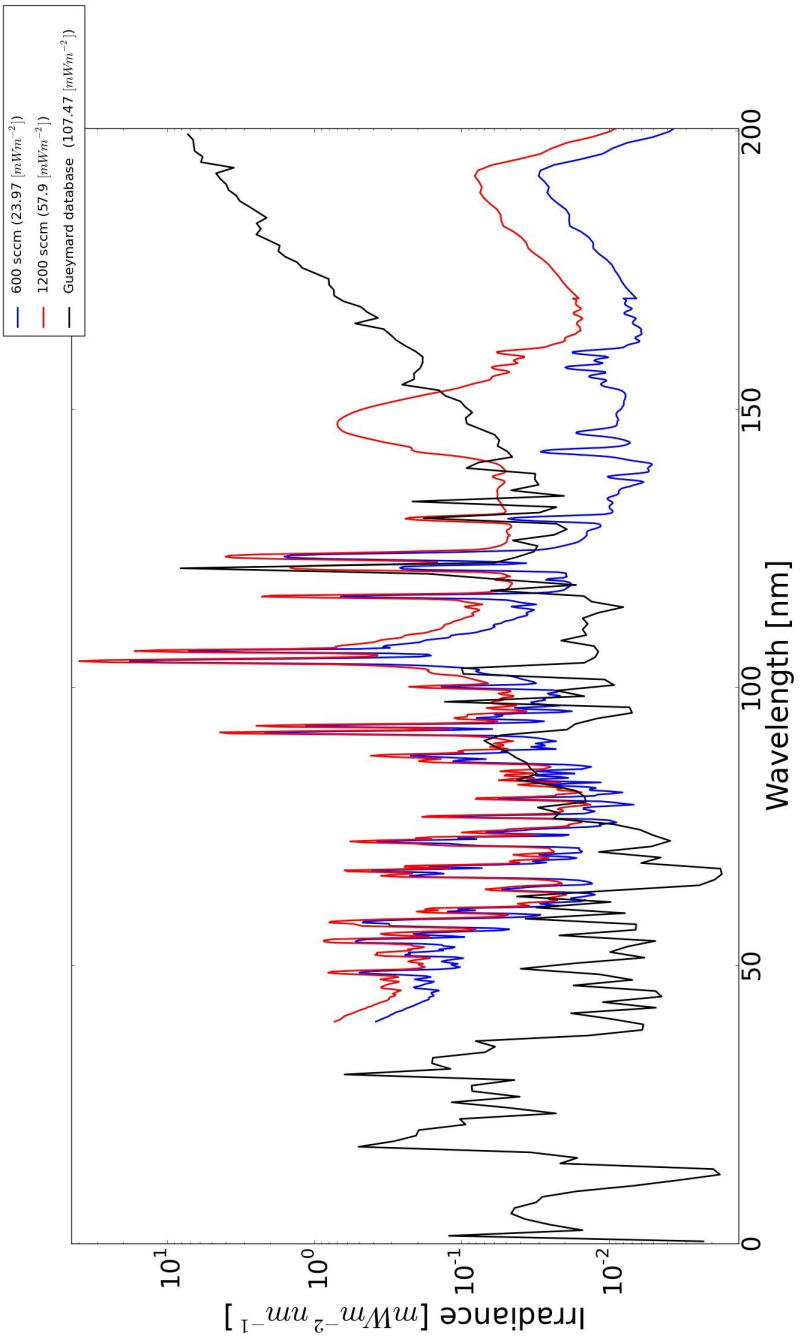

Figure 11: The spectra of the VUV-simulator for different gas flows (600 and 1200 sccm) comparing to the Gueymard database denoted as a black line. The given total intensity of the solar spectrum taken from the Gueymard database is calculated from 40 nm to 200 nm and it is shown in the legend.

and a gas flow of 1200 sccm (see Table 4.1). The integral of the VUV-simulator's irradiance can reach: 26.3 SC for a gas flow of 1200 sccm, 12.5 SC for a gas flow of 600 sccm and 3 SC for a gas flow of 300 sccm in the wavelength range from 40 nm to 120 nm. Fig. 11 shows the spectra of the VUV-simulator for two different gas flows 600 and 1200 sccm. There is plotted the solar spectrum of the Gueymard database for comparison too. The solar spectral intensity is larger than that of the VUV-simulator at wavelengths higher than 150 nm.

The spectral distribution of the accelerating factors is presented in Fig. 12. The spectral intensity distribu-

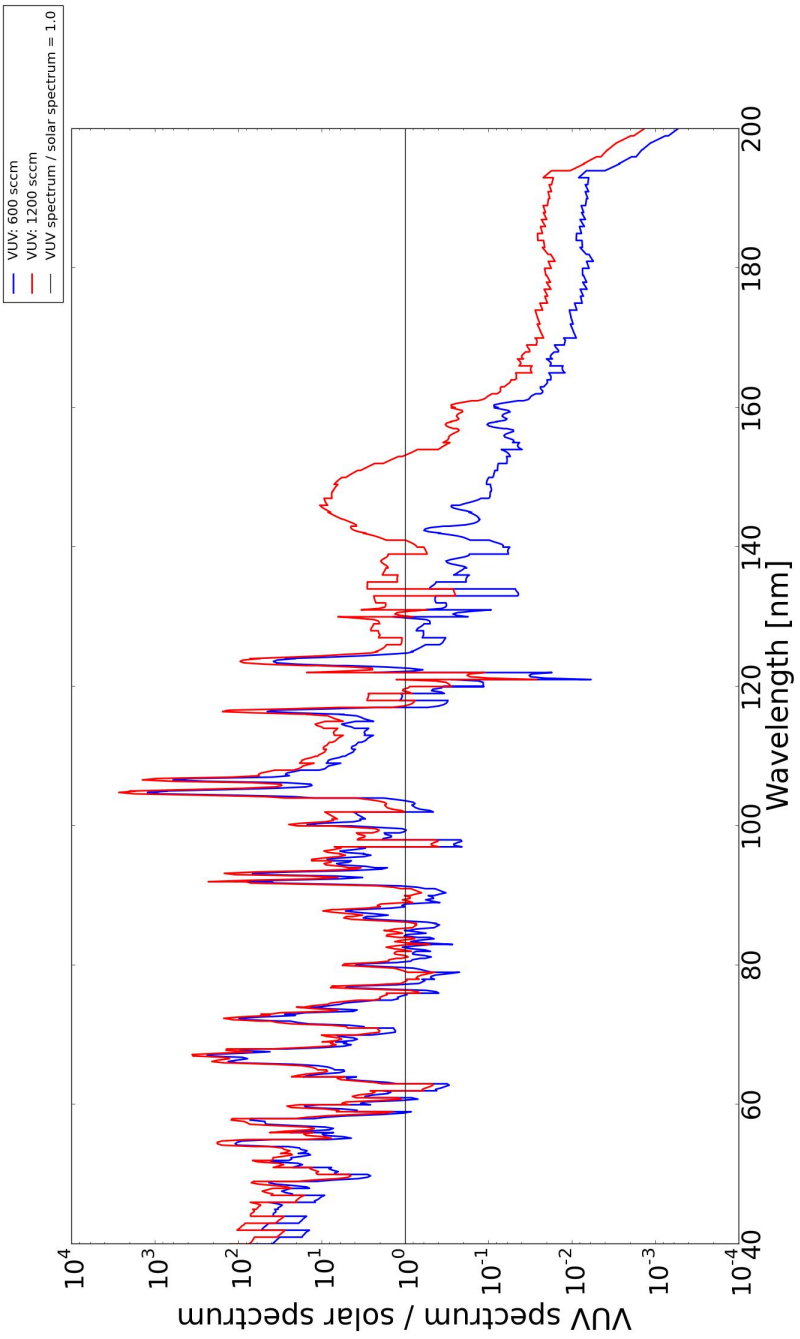

Figure 12: VUV spectra for gas flows of 600 and 1200 sccm divided by the spectrum of the Sun taken from the Gueymard database (Gueymard, 2004).

tions of the VUV-simulator are divided by the solar ones taken from the Gueymard database for two representative gas flows. The acceleration factor is significantly larger than 1 in almost the complete range up to 120 nm. For wavelengths higher than 115 nm, a Deuterium lamp yields higher intensities and sufficiently large acceleration factors. Depending on the specific purposes of experiments to determine degradation effects of materials exposed to VUV radiation, the appropriate gas flow has to be chosen.

Table 4.1: The differential values of the Gueymard's and VUV-simulator's spectral intensities as well as acceleration factors in bins of 10 nm. Unfortunately, there is no matchable spectrum for a gas flow of 300 sccm in the wavelength range of $120 - 160$ nm.

Wavelength	Gueymard	300 sccm		600 sccm		1200 sccm	
nm	mW m^{-2}	mW m^{-2}	Acc.	mW m^{-2}	Acc.	mW m^{-2}	Acc.
40-50	0.11	0.69	6.27	2.23	20.27	4.05	36.82
50-60	0.14	0.62	4.43	1.85	13.21	3.09	22.07
60-70	0.11	0.28	2.55	0.69	6.27	1.08	9.82
70-80	0.13	0.19	1.46	0.49	3.77	0.79	6.08
80-90	0.33	0.14	0.42	0.42	1.27	0.76	2.30
90-100	0.37	0.63	1.70	1.85	5.00	3.74	10.11
100-110	0.31	2.51	8.10	13.11	42.29	29.56	95.35
110-120	0.21	0.07	0.33	0.07	3.33	1.93	9.19
120-130	8.58	-	-	1.77	0.21	5.24	0.61
130-140	0.67	-	-	0.12	0.18	0.70	1.04
140-150	0.69	-	-	0.11	0.16	4.02	5.83
150-160	1.65	-	-	0.11	0.07	1.46	0.88
160-170	3.60	0.01	2.78×10^{-3}	0.08	0.02	0.22	0.06
170-180	11.09	0.01	9.02×10^{-4}	0.08	7.21×10^{-3}	0.21	0.02
180-190	26.01	0.02	7.69×10^{-4}	0.18	6.92×10^{-3}	0.53	0.02
190-200	53.47	0.02	3.74×10^{-4}	0.19	3.55×10^{-3}	0.53	0.01

Table 4.2: The integrated values of the Gueymard's and VUV-simulator's spectral intensities as well as acceleration factors with fixed lower limit of the wavelength range (40 nm). Unfortunately, there is no matchable spectrum for a gas flow of 300 sccm in the wavelength range of $120 - 160$ nm.

Wavelength	Gueymard	300 sccm		600 sccm		1200 sccm	
nm	mW m^{-2}	mW m^{-2}	Acc.	mW m^{-2}	Acc.	mW m^{-2}	Acc.
40-50	0.11	0.69	6.27	2.23	20.27	4.05	36.82
40-60	0.25	1.31	5.24	4.08	16.32	7.14	28.56
40-70	0.36	1.59	4.42	4.77	13.25	8.22	22.83
40-80	0.49	1.78	3.63	5.26	10.73	9.01	18.39
40-90	0.82	1.92	2.34	5.68	6.93	9.77	11.91
40-100	1.19	2.55	2.14	7.52	6.32	13.51	11.35
40-110	1.50	5.06	3.37	20.64	13.76	43.07	28.71
40-120	1.71	5.13	3.00	21.33	12.47	45.00	26.32
40-130	10.29	-	-	23.11	2.25	50.25	4.88
40-140	10.96	-	-	23.22	2.12	50.95	4.65
40-150	11.65	-	-	23.33	2.00	54.97	4.72
40-160	13.30	-	-	23.44	1.76	56.43	4.24
40-170	16.90	-	-	23.52	1.39	56.64	3.35
40-180	27.99	-	-	23.60	0.84	56.86	2.03
40-190	54.00	-	-	23.78	0.44	57.39	1.06
40-200	107.47	-	-	23.98	0.22	57.92	0.54

4.3. The stability of the radiation intensity of the VUV-simulator

The presumption of the variability of the radiation intensity, as seen during the calibration campaign, has been confirmed by the stability analysis. In order to get an idea about the stability, several measurements with identical settings of gas flow and electron current has been performed at different days and different operating times after the regeneration of the source during the calibration process at PTB.

The stability is affected by different effects which may compensate each other, at least partially. One effect is the formation of ice at the cold baffles around the light spot. The growing lumps of ice decrease the pumping power. Therefore, the intensity could increase because the gas density increases. It has to be mentioned, that this increase of intensity is mostly seen in measurements performed at the same day, however, not always and not in the full spectral range. On the other hand, the apertures at the cold baffles for the electron beam and for the light outlet will freeze up at longer operating time. That may cause a decrease of intensity. It will be reduced by the lower and/or defocussed electron beam and/or the lower solid angle of the out-coming light. Other the stability influencing effects are a small variation of both the gas flow and the electron current.

Due to the small number of comparable measurements a complete statistical analysis was not feasible. Instead, a worst case estimation has been performed as follows.

The stability of the VUV-simulator has been estimated by comparing the intensity spectra taken at almost identical settings but made at as far as possible distant moments in time. The different number of measurements at each spectral range ($40 - 135$ nm: 3; $135 - 220$ nm: 9; $220 - 330$ nm: 5; $330 - 410$ nm: 5) was taken into account to determine the mean value. The maximum deviation

was calculated by division of the maximum respectively the minimum intensity by the mean value at each wavelength. The results are shown in Fig. 13 only for the gas flow of 1200 sccm.

The lowest deviation to the average signal of +/- 10% appears in the wavelength range from 40 nm to 105 nm. Above 105 nm to 135 nm are bands where the deviation is +/- 20% (see upper left plot). The highest one of −50% is in the wavelength range of 145 nm to 155 nm, while in the range of 160 nm to 220 nm the deviation is +/-25% (see upper right plot). In the ranges of 220 nm to 330 nm and 330 nm to 410 nm the deviation from the average signal is equal or less than +/- 20% (see lower left and right plot).

The analysis of the plots in Fig. 13 shows an increase of the maximum deviation in the higher wavelength ranges. This result is influenced by the different number of measurements too. Nevertheless, it is acceptable in the range of short wavelengths. This stability analysis shows that the VUV simulator is not qualified as a calibration standard, i.e. for detector calibration. However, the stability in the VUV range is sufficient to perform irradiation tests for material investigations. The larger deviations in higher wavelength ranges are not a serious problem since the intensity there is at least one order of magnitude smaller than in the range below 115 nm see Figs 10 and 11. The very low intensity of the VUV-simulator at wavelengths larger than 115 nm is in the CIF compensated by the Deuterium lamp. It exceeds for wavelengths > 115 nm the solar intensity by about one order of magnitude.

5. Summary

Short wavelength electromagnetic radiation as generated by the VUV-simulator plays a crucial role in space material science due to photoionization and photodissociation effects (see Section 1). The maximum acceleration factor reached at the wavelength range from 40 nm to 120 nm is about 26.3 SC at a gas flow of 1200 sccm. In the same range but at a gas flow of 600 sccm the acceleration factor is 12.5 SC. With the smallest gas flow used in the calibration procedure (300 sccm) the factor is about 3 SC. Since the source has many operational parameters (see Section 2), changes of the gas flow will cause variations of the acceleration factor. Given an operating time of at least 8 h and the large acceleration factors, the VUV-simulator is a suitable facility for various material tests and degradation experiments.

The simulator passed the first campaign of the calibration procedure. The spectral lines are calibrated from 40 nm to 410 nm. Based on the experiences made with first VUV-simulator (Verkhovtseva at al., 1997) a significant intensity down to 5 nm can be expected, i.e. this source would cover also the soft X-ray range of the solar spectrum. Therefore a second calibration campaign for wavelengths smaller than 40 nm is necessary. It can be performed at the recently set-up facility for source calibration at the Metrology Light Source of PTB (MLS) (Gottwald et al., 2012).

The calibration procedure has proved that the VUV-simulator meets the requirements with respect to the solar spectral intensity distribution, the achievable acceleration factors, and the size of the irradiated area.

The stability analysis of the VUV-simulator signal shows that the maximum intensity deviations in the VUV range below 115 nm are in the order of 10%. The larger deviation for wavelengths above 115 nm are not a serious problem for material testing in the CIF because the VUV-simulator intensity in that range is negligible small and the Deuterium lamp is used (see Section 4.3). Therefore, a satisfactory operation of the VUV-simulator can be expected. Nevertheless, in a forthcoming calibration campaign the stability will be subject of a more systematic analysis.

6. Acknowledgements

We want to acknowledge the big help of Simone Kroth and Wolfgang Paustian at their assistance in performing all the measurements for conditioning and calibrating the source.

Appendix A. Tabulated spectra lines

Table A.1 contains validated spectra lines and their elements in the wavelength range from 40 to 410 nm. The continuous spectrum in the wavelength range from 138 to 160 nm is presented in the Table A.2. All of the spectra lines and their elements are taken from the NIST database (Ralchenko et al., 2011).

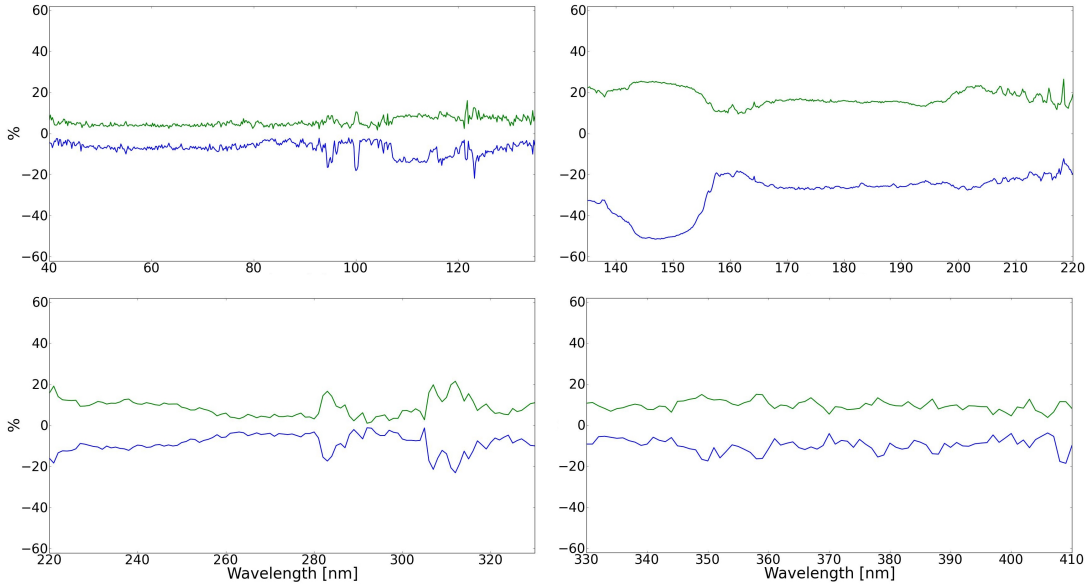

Figure 13: The maximum deviation (green line positive, blue line negative) of the spectral intensity distribution in the four spectral ranges related to their mean value.

References

Agnolan, D., Study Overview of a Solar Sail Demonstrator: Geosail, SCI-PA, 1, 2007, 1 - 54

ASTM, E 490-00a, Solar Constant and Zero Air Mass Solar Spectral Irradiance Tables, reapproved 2006

ASTM, E512 - 94(2010), Standard Particle for Combined, Simulated Space Environment Testing of Thermal Control Materials with Electromagnetic and Particulate Radiation, 2010

Curdt W., Landi E., Feldman U., The SUMER Spectral Atlas of Solar Coronal Features, Astronomy and Astrophysics, 427, 2004, 1045

Dachwald B., Potential Solar Sail Degradation Effects on Trajectory Design, AIAA Conference, San Diego California, 7 - 11 August 2005

ECSS-Q-ST-70-06C: Particle and UV Radiation Testing for Space Materials, 2008

Gottwald A., Klein R., Mueller R.M., Richter M., Scholze F., Thornagel R., Ulm G., Current capabilities at the Metrology Light Source, Metrologia 49, 2012, 146-151.

Gueymard Ch.A., The Sun's Total and Spectral Irradiance for Solar Energy Applications and Solar Radiation Models, 76, 2004, 423 - 453

Heltzel S., Semprimoschnig C. O. A., van Eesbeek M. R. J., Environmetal Testing of Thermal Control Materials at Elevated Temperature and Intense Ultraviolet Radiation, Journal of Spacecraft and Rockets, 46, 2009, 248 - 254

Lura F., Hagelschuer D., Glotov A.I., Tschaly Y., Experiments in the Test Facility KOBE for the Investigation of Degradation Effects of Thin Foil Samples for a Solar Sail Mission Concerning the Simultaneous Influence of Space Environment Properties, 2002, 22nd Space Simulation Conference

Marco J., Remaury S., Evaluation of Thermal Control Coatings Degradation in Simulated GEO-space Environment, High Performance Polymers 16, 2004, 177

Marco J., Remaury S., Tonon C., Eight Years GEO Ground Testing of Thermal Control Coatings, 11th International Symposium on Materials in a Space Environment, Aix-En-Provence, France (2009),

Polsak A., Eesbeek M., Semprimoschnig C. O. A., In-situ testing at ESTES's SORASI facility, Proceedings of the 9th International Symposium on Materials in a Space Environment, ESA, Noordwijk, 2003

Ralchenko, Yu., Kramida, A.E., Reader, J., and NIST ASD Team (2011). NIST Atomic Spectra Database (v. 4.1.9), [Online]. Available: http://physics.nist.gov/asd [2012, May 29]. National Institute of Standards and Technology, Gaithersburg, MD.

Redhead P. A., Hydrogen in Vacuum Systems: An Overview, Hydrogen in Materials & Vacuum Systems, 2002, 243

Renger T., Witzke A., Sznajder M., Geppert U., The DLR Complex Irradiation Facility (CIF), 12th International Symposium on Materials in the Space Environment (ISMSE-12), ESA, Noordwijk, 2012

Renger T., Sznajder M., Witzke A., Geppert U., The Complex Irradiation Facility at DLR-Bremen, Advances in Solar Sailing, Springer Praxis Books, 2014

Richter M., Hollandt J., Kroth U., Paustian W., Rabus H., Thornagel R., Ulm G., The Two Normal-Incidence Monochromator Beam Lines of PTB at BESSY II, Nuclear Instruments and Methods in Physics Research A, 467 - 468, 2001, 605 - 608

Richter M., Ulm G., Radiometry Using Synchrotron Radiation at PTB, Journal of Electron Spectroscopy and Related Phenomenena, 101 - 103, 1999, 1013 - 1018

Romero M., Boscher D., Experimental Models of Effects Simulation, ESA Workshop on Space Wether, ESA Space Environments and Effects Analysis Section (ESA TOS-EMA), ESTEC, Noordwijk, The Netherlands, 1998.

Sharma A.K., Sridhara N., Degradation of Thermal Control Materials Under a Simulated Radiative Space Environment, J. Adv. Space Res., 2012

Verkhovtseva E.T, Yaremenko V.I., Telepnev, Lura F., Gas-jet Simulator of Solar VUV and Soft X-ray Radiation and Irradiation Effect on Some Material, Proceedings of the 7th International Symposium on Materials in Space Environment, Toulouse, France (1997)

Table A.1: Validated spectra lines in the wavelength range from 40 to 410 nm. The lines are depicted in Figs. 6, 7, 8 and 9. Data are taken from the NIST database (Ralchenko et al., 2011).

Wavelength [nm]	Element	Wavelength [nm]	Element	Wavelength [nm]	Element
46.201	Ar VI	104.822	Ar I	248.00368	W II
47.575	Kr V	106.6134	Cu II	252.00734	W II
48.799	Ar IV	108.592	Al V	253.99098	W II
50.109	Ar VII	109.4264	W IV	257.98438	Fe I
50.782	Kr VI	111.322	Cu V	261.9954	W I
52.2186	He I	111.9947	Cu II	264.998	W I
54.383	Ar VI	114.6102	W III	268.0046	W I
55.775	Kr IV	116.4867	Kr I	271.0004	W I
57.8212	Kr III	119.4528	Ar V	276.0036	W I
59.7701	Ar II	121.56699	HI	283.0054	Fe I
60.183	Kr IV	123.62	Cr III	288.99877	Fe I
61.1831	Kr IV	128.395	Ar VI	294.5106	He I
62.165	Ar VII	130.387	Ar VI	297.9860	W I
63.72881	Ar III	132.3847	W IV	300.0	Fe I
66.200	Ar IX	134.3710	Ar III	303.01481	Fe I
67.0948	Ar II	135.6086	W III	309.0088	W I
67.897	Kr IV	137.9670	Al III	314.0146	W I
68.8915	Kr VII	139.3886	W III	321.01863	Fe I
69.9812	Kr IV	142.3889	W V	324.993	Mo I
72.394	Ar VII	145.8088	W IV	334.97241	Fe I
73.0	Fe III	149.1151	W III	337.997	Mo I
74.011	Ar VIII	154.3841	W IV	343.003	Ar III
76.8132	Kr III	155.982	Ar IV	348.983	O IV
78.216	Kr IV	157.592	La IV	350.98614	Fe I
80.109	Ar IV	158.8466	W III	356.006	W I
82.598	Kr VI	160.3074	Ar II	357.995	Kr III
83.417	Kr VI	162.790	Kr IV	364.0134	W I
84.2805	Ar I	165.5639	Cr V	365.97333	Fe I
85.0154	Kr I	167.211	Kr IV	367.99131	Fe I
86.832	Ar IV	169.028	Cr III	372.999	W I
87.792	Ar VII	178.5729	W III	377.03012	Fe I
89.394	Kr IV	183.001	Ni III	380.9848	W I
90.0313	Kr I	188.77646	Fe I	384.99664	Fe I
91.9342	H I	192.0378	W III	386.9928	W I
93.0749	H I	197.39162	Fe I	393.0231	W I
94.9742	H I	206.3848	W IV	397.98498	W II
96.4075	Kr IV	213.20171	Fe I	403.9938	Fe I
97.2541	H I	217.80806	Fe I	407.98377	Fe I
98.03	Ar IV	223.008	Cu I		
99.004	Ar IV	228.998	Ni I		
100.1883	W IV	232.003	Ni I		
102.5948	W IV	241.9985	W II		

Table A.2: Validated spectra lines in the wavelength range from 138 to 160 nm. The lines are depicted in Fig. 7 for a gas flow of 1200 and 2000 sccm. Data are taken from the NIST database (Ralchenko et al., 2011).

Wavelength [nm]	Element	Wavelength [nm]	Element	Wavelength [nm]	Element	Wavelength [nm]	Element
138.0723	Ar II	144.766	Ar V	152.411	Kr IV	157.5375	Kr II
138.2228	Ar II	144.835	Ar IV	152.515	Kr IV	157.566	Kr IV
138.235	Kr V	145.1879	Ar II	152.5486	Kr II	157.5815	Ar II
138.2765	Ar II	145.226	Kr V	152.566	Kr IV	157.594	Kr IV
138.386	Kr V	145.348	Kr III	152.626	Ar IV	157.6155	Kr II
138.459	Kr V	145.544	Ar IV	152.795	Ar IV	157.65915	Ar III
138.511	Kr IV	145.5484	Ar II	152.818	Ar IV	157.6897	Ar II
138.681	Kr IV	145.630	Kr IV	153.250	Kr III	157.8812	Ar II
138.900	Kr IV	145.730	Kr IV	153.286	Kr IV	157.9513	Kr II
138.996	Kr IV	145.923	Ar IV	153.341	Kr IV	157.9731	Kr II
139.212	Ar XI	145.948	Kr IV	153.553	Kr IV	157.974	Kr IV
139.263	Kr V	145.9875	Ar II	153.600	Ar IV	158.0260	Ar III
139.361	Kr V	146.00973	Ar III	153.668	Ar IV	158.0768	Ar II
139.564	Ar IV	146.02487	Ar II	153.855	Kr V	158.0960	Ar II
139.6231	Ar II	146.099	Ar IV	153.9075	Kr II	158.198	Kr IV
140.089	Kr IV	146.109	Kr IV	154.007	Kr V	158.248	Kr III
140.168	Kr III	146.265	Kr XXIII	154.026	Ar IV	158.30377	Ar III
140.181	Kr IV	146.3	Ar VIII	154.2540	Ar III	158.383	Ar II
140.220	Kr V	146.3155	Ar II	154.291	Kr V	158.4563	Kr II
140.288	Kr III	146.4072	Kr II	154.4177	Ar II	158.601	Kr III
140.750	Ar IV	146.4176	Ar II	154.4711	Ar II	158.6093	Kr II
140.930	Ar IV	146.5153	Ar II	154.508	Kr IV	158.6170	Kr II
141.013	Ar IV	146.553	Kr IV	154.630	Kr IV	158.6256	Ar II
141.157	Kr IV	146.55506	Ar III	164.666	Ar IV	158.6330	Ar III
141.235	Kr III	146.57036	Ar III	154.7354	Ar II	158.66206	Ar III
141.3894	Kr II	146.600	Kr IV	155.452	Ar IV	158.6621	Kr II
141.397	Ar V	146.614	Kr IV	155.539	Kr V	158.8740	Ar III
141.614	Kr V	146.6460	Kr II	155.6220	Ar III	158.9384	Kr II
141.689	Kr IV	146.6524	Ar II	155.6630	Ar III	158.9463	Ar II
141.959	Ar IV	146.78533	Ar III	155.7302	Ar II	158.987	Kr IV
142.060	Ar VI	146.8006	Ar III	155.851	Kr IV	159.0229	Ar II
142.070	Kr III	146.8021	Kr II	155.8802	Kr III	159.032	Kr IV
142.171	Kr IV	147.204	Ar IV	155.9072	Ar II	159.160	Kr III
142.2000	Ar III	147.2594	Ar II	155.982	Ar IV	159.1933	Ar II
142.251	Ar VI	147.448	Ar IV	156.0184	Ar II	159.2565	Kr II
142.2512	Kr II	147.4537	Ar II	156.193	Kr IV	159.3581	Ar II
142.3553	Kr III	147.717	Kr IV	156.2441	Ar II	159.386	Kr IV
142.429	Kr IV	147.915	Ar IV	156.285	Kr III	159.3946	Kr II
142.497	Kr V	148.136	Kr IV	156.3036	Ar II	159.4787	Ar II
142.575	Kr III	148.160	Ar IV	156.5377	Ar II	159.4895	Kr II
142.619	Ar IV	148.3429	Kr III	156.603	Kr V	159.5734	Ar II
142.777	Kr III	148.601	Ar IV	156.6812	Ar II	159.6141	Ar II
142.965	Kr IV	148.628	Kr IV	156.7987	Ar II	159.6210	Ar III
142.984	Kr V	148.952	Kr IV	156.8050	Kr II	159.641	Kr IV
143.068	Kr IV	149.018	Kr IV	156.8690	Ar III	159.667	Kr IV
143.378	Kr V	149.0928	Kr II	156.891	Kr V	159.8082	Kr II
143.4070	Ar III	149.1104	Kr II	156.9135	Kr II	159.8561	Ar II
143.5085	Kr II	149.532	Ar IV	156.982	Kr IV	159.8724	Ar II
143.557	Ar IV	149.5769	Kr II	156.9886	Kr III	159.8872	Ar II
143.5676	Kr II	149.781	Ar IV	157.017	Ar IV	159.9125	Ar II
143.620	Kr V	149.828	Kr V	157.038	Kr IV	159.9492	Kr II
143.648	Kr IV	149.850	Kr III	157.1390	Ar II	159.9597	Ar II
143.7020	Ar III	149.964	Kr V	157.1876	Kr II	159.98	Kr V
143.7170	Ar III	150.0740	Ar III	157.1920	Ar III	159.982	Kr IV
143.912	Kr IV	150.158	Kr IV	157.23340	Ar III		
144.007	Ar III	150.290	Kr IV	157.2340	Kr II		
144.0210	Ar III	150.591	Kr III	157.3050	Ar III		
144.2440	Ar III	150.880	Ar IV	157.318	Kr III		
144.343	Kr IV	150.984	Ar IV	157.3404	Kr II		
144.4	Ar VIII	151.351	Kr IV	157.4103	Kr II		
144.4343	Kr II	151.4585	Kr II	157.4340	Kr II		
144.528	Kr IV	151.605	Ar IV	157.4402	Ar II		
144.563	Kr IV	151.685	Kr IV	157.4733	Kr II		
144.750	Kr III	152.162	Kr IV	157.498	Kr IV		
144.762	Kr IV	152.371	Kr IV	157.4992	Ar II		